Fabrication of Electrospun Poly(L-Lactide-co-ε-Caprolactone)/Collagen Nanoyarn Network as a Novel, Three-Dimensional, Macroporous, Aligned Scaffold for Tendon Tissue Engineering

Yuan Xu, BS,[1,2] Jinglei Wu, MS,[3] Haoming Wang, BS,[1,2] Hanqin Li, BS,[1,2] Ning Di, BS,[1,2] Lei Song, BS,[1,2]
Sontao Li, MS,[1,2] Dianwei Li, MS,[1,2] Yang Xiang, MS,[4] Wei Liu, BS,[3]
Xiumei Mo, PhD,[3] and Qiang Zhou, PhD[1,2]

Tissue engineering techniques using novel scaffolding materials offer potential alternatives for managing tendon disorders. An ideal tendon tissue engineered scaffold should mimic the three-dimensional (3D) structure of the natural extracellular matrix (ECM) of the native tendon. Here, we propose a novel electrospun nanoyarn network that is morphologically and structurally similar to the ECM of native tendon tissues. The nanoyarn, random nanofiber, and aligned nanofiber scaffolds of a synthetic biodegradable polymer, poly(l-lactide-co-ε-caprolactone) [P(LLA-CL)], and natural collagen I complex were fabricated using electrospinning. These scaffolds were characterized in terms of fiber morphology, pore size, porosity, and chemical and mechanical properties for the purpose of culturing tendon cells (TCs) for tendon tissue engineering. The results indicated a fiber diameter of 632 ± 81 nm for the random nanofiber scaffold, 643 ± 97 nm for the aligned nanofiber scaffold, and 641 ± 68 nm for the nanoyarn scaffold. The yarn in the nanoyarn scaffold was twisted by many nanofibers similar to the structure and inherent nanoscale organization of tendons, indicating an increase in the diameter of 9.51 ± 3.62 μm. The nanoyarn scaffold also contained 3D aligned microstructures with large interconnected pores and high porosity. Fourier transform infrared analyses revealed the presence of collagen in the three scaffolds. The mechanical properties of the sample scaffolds indicated that the scaffolds had desirable mechanical properties for tissue regeneration. Further, the results revealed that TC proliferation and infiltration, and the expression of tendon-related ECM genes, were significantly enhanced on the nanoyarn scaffold compared with that on the random nanofiber and aligned nanofiber scaffolds. This study demonstrates that electrospun P(LLA-CL)/collagen nanoyarn is a novel, 3D, macroporous, aligned scaffold that has potential application in tendon tissue engineering.

Introduction

TENDONS are connective tissues that transmit tensile forces and provide connective flexibility between muscles and bones. Tendons possess a hierarchical structure composed of collagen fiber bundles arranged along their longitudinal axes.[1] Tendon injuries are frequently reported, especially among individuals engaged in physical activity.[2] However, native tendons have a limited capacity for healing, presenting the formidable challenge of tissue regeneration after injury. Developments in tissue engineering may provide a promising treatment for tendon injuries.[3] Biological materials play a key role as scaffolds; these materials commonly provide synthetic extracellular matrix (ECM) environments and three-dimensional (3D) templates for tissue regeneration.[4] Ideal tendon tissue engineering scaffold materials should exhibit good biocompatibility and biodegradability, strong mechanical properties, high porosity, adjustable pore sizes, and the ability to mimic the basic structures and ECM environments of native tendons to promote cell growth and tissue formation.[5,6] Both natural (collagen,[7] chitin,[8] and silk[9]) and biodegradable synthetic [poly(lactic acid),[10] poly(lactide-co-glycolide),[11] and poly (glycolic acid)[12]] materials have been used as fibrous

---

[1]Department of Orthopaedics, Southwest Hospital, Third Military Medical University, Chongqing, China.
[2]National and Regional United Engineering Laboratory of Tissue Engineering, Southwest Hospital, Third Military Medical University, Chongqing, China.
[3]College of Chemistry and Chemical Engineering and Biological Engineering, Donghua University, Shanghai, China.
[4]Medical Research Center, Southwest Hospital, Third Military Medical University, Chongqing, China.

scaffolds for tendon regeneration. Although past studies have produced promising results, the scaffold architectures differ from the structure and inherent nanoscale organization of native tendons.[13] In addition, these scaffolds do not have an adequate 3D porous architecture that allows for the infiltration of seeding cells. As an essential step in tissue regeneration, cellular infiltration should allow for tissue integration in scaffolds.

Electrospinning is a uniquely simple and adaptable method for engineering scaffolds. The scaffolds fabricated by electrospinning exhibit high porosity and micro- to nano scale topography, similar to the structure of natural ECM,[14] and are widely used in the engineering of various tissues, including vascular tissues, myocardial tissues, bone, skin, cartilage, and tendons/ligaments.[15–20]

With its high elasticity and capacity for recovery from elastic deformation, poly(l-lactide-co-ε-caprolactone) [P(LLA-CL)] copolymer is often applied as a mechanostimulating tissue engineering scaffold for tendon/ligament,[20,21] blood vessel,[22] and cartilage[23] engineering applications. The biodegradable copolymer P(LLA-CL) (50:50) could be useful as a provisional functional scaffold in muscular and cardiovascular tissue engineering.[24] However, the surface of P(LLA-CL) lacks the adhesive proteins and structural proteins that would typically play key roles in cell adhesion, cell proliferation, and tissue remodeling.[25] Collagen, a protein prevalent in natural ECM, is attractive as a component of tissue engineering scaffold because it is the most commonly used multifunctional substrate for promoting cell proliferation and differentiation.[26] Previous research has revealed that the scaffolds fabricated by electrospinning mixed polymer solutions exhibit better biological properties than those of synthetic polymer scaffolds and better mechanical properties than those of natural polymer scaffolds.[27,28] Thus, we selected P(LLA-CL) and collagen as the raw materials for manufacturing scaffolds.

Successful tissue engineering scaffolds should be conducive to the penetration of specific cells and should have characteristics that promote the functional expression of penetrating cells. Traditional electrospun scaffolds entirely consist of nanofiber layers tightly packed through a sheet-like assembly process; such scaffolds can only provide a superficial pore structure, and they hinder the infiltration and growth of cells.[29] Nanoyarn networks, which are fabricated as suspensions in water, form loose, dispersed nanofibers through a novel dynamic flow collecting system during the electrospinning process. These nanoyarn networks retain a good porous microstructure after freeze drying and thus are beneficial for cell penetration.[30] The nanoyarn networks have been fabricated from various polymers, including poly(vinylidene difluoride)[31] and poly(ε-caprolactone).[32] However, very few studies have focused on the differences in the structural and biological properties between novel nanoyarn scaffolds and traditional electrospun nanofiber scaffolds of identical composition or provided testimonies showing the great application potential of nanoyarn scaffolds in tendon tissue engineering.

Here, we fabricated 3D networks of electrospun nanoyarn scaffold with aligned microstructures, large pores, and high degrees of porosity using this novel electrospinning method. The scaffold was composed of P(LLA-CL) and Type I collagen, which morphologically and structurally mimicked the ECM of native tendon tissues. Moreover, we sought to characterize the infiltration and the specific gene expression of the tendon cells (TCs) that were seeded on the nanoyarn networks. As a control, we used a traditional electrospinning method to manufacture random nanofiber and aligned nanofiber scaffolds of the same composition. We evaluated the morphology, porosity, components, and mechanical properties of the scaffolds and the cell attachment, proliferation, infiltration, and expression of tendon-specific ECM genes on the scaffold. Notably, this study demonstrates that these blended nanoyarn scaffolds satisfy the requirements for functional tendon tissue engineering.

Materials and Methods

Materials

P(LLA-CL) (LA:CL = 50:50, Mw = 300,000) was provided by Nara Medical University. Type I collagen was obtained from Sichuan Ming-Rang Bio-Tech Co. Ltd. and 1,1,1,3,3,3-hexafluoro-2-propanol (HFIP) [for dissolving P(LLA-CL) and collagen] from Da-Rui Co. Ltd.

Scaffold fabrication

Nanoyarn scaffolds studied were fabricated by electrospinning using a dynamic liquid supporting system as previously described,[31] with some modifications. Briefly, a hole (8 mm in diameter) was created in a basin, thereby allowing the flow of water to form a water vortex. A pump was employed to recycle water back to maintain the water level after the water was drained through the hole into a tank below the basin. P(LLA-CL) and collagen were dissolved in HFIP, yielding a 90:10 blended solution (8 w/v%). The blended solution jet rate, located 15 cm above the water vortex, was 1.0 mL/h under a high voltage of 15 kV. As the HFIP evaporated, electrospun nanofibers were generated and deposited on the water; then, the nanofibers were twisted into a bundle of nanoyarn in the water vortex and collected by a rotating mandrel (60 r/min) to form a nanoyarn scaffold. After being removed from the mandrel, the nanoyarn scaffold was frozen at −80°C for 2 h and subsequently freeze-dried overnight. The final nanoyarn scaffold was ∼150 μm thick, composed of aligned nanoyarn, and stored in a vacuum oven. To fabricate a randomly oriented nanofiber scaffold, the same composition of blended solution as that described for the electrospinning process for nanoyarn scaffolds was prepared and fed by a syringe. A flat fabric was used to collect the random nanofibers 15 cm from the blunt tip. When the aligned nanofiber scaffold was manufactured, the flat fabric was replaced by a rotating collecting target to collect the nanofibers 15 cm from the blunt tip. All nanofiber scaffolds used in this study were ∼100 μm thick.

Morphology and characterization of P(LLA-CL)/ collagen random nanofiber, aligned nanofiber, and nanoyarn scaffolds

Scaffold morphology. The scaffold samples were examined by scanning electron microscopy (SEM) (Hitachi, S-3400N). The angle distribution (relative to the vertical axis), diameter, and pore sizes of the specimens were determined from SEM images using Image J 1.45s image visualization software. The angle distribution and average diameter were

measured from $\sim$100 random nanofibers in the SEM images. The average pore size was determined from $\sim$50 pores in a typical SEM image ($n=3$).

Scaffold porosity. The exact sizes of scaffold samples were estimated using a Vernier caliper, and the volumes (V) of the scaffolds were measured. The dry scaffolds were weighed (W_d), submerged in absolute ethanol with a density of r for 2 h, and weighed again (W_s). The porosity was calculated as $(W_s - W_d)/r/V$, ($n=3$).

Fourier transform infrared spectroscopy. The chemical analysis of collagen, P(LLA-CL), and the P(LLA-CL)/collagen random nanofiber, aligned nanofiber, and nanoyarn scaffolds was performed using attenuated total reflectance-Fourier transform infrared spectroscopy (FTIR) over the range of 2000–800 cm^{-1}.

Cell isolation and culture

Primary TCs were harvested from the bilateral tendon of Oryctolagus cuniculus (6–8 weeks old, 2.0–2.5 kg), isolated according to previously described procedures,[27] and then expanded in Dulbecco's modified Eagle's medium (DMEM)/F12 (1:1) (HyClone) medium containing 10% foetal bovine serum (Invitrogen), 1% penicillin, and streptomycin (HyClone). Upon reaching confluence, TCs were trypsinized by 0.25% trypsin (HyClone) and passaged.

The three groups of scaffold samples (length×width: 10×10 mm) were placed in 24-well tissue-culture polystyrene plates (TCPSs; Costar) and sterilized with 70% ethanol for 30 min. The scaffold samples were then rinsed five times with sterile phosphate-buffered saline (PBS), 15 min each time, and subsequently immersed in DMEM/F12 medium overnight. The TCs (passage 3) were seeded on the scaffolds (1×10^5 cells/scaffold). The empty wells of the 24-well TCPSs served as a control. After planting TCs onto the scaffolds, the cell-seeded scaffolds were stored in an incubator (37°C, 5% CO_2) for 4 h to promote cell adhesion. Then, the culture medium was added into the wells and changed every other day.

Cell adhesion and proliferation

The viability of TCs on the scaffold samples and TCPS controls was determined using the commercially available Cell Counting Kit-8 (CCK-8; Beyotime). A cell adhesion test was performed 4 h after cell seeding. For the cell proliferation assay, the tests were conducted on days 1, 7, and 14. The medium was removed from the 24-well TCPSs at each time point, and fresh medium containing 10% CCK-8 was added for 3 h of incubation. The absorbance was measured at 450 nm using a microplate reader (Model 550; Bio-Rad). The corresponding number of cells as correlated to optical density and calculated by comparing with a standard curve ($n=3$).

Cell morphologies on scaffolds imaged by SEM

The morphologies of TCs on the scaffold samples were examined using SEM at 4 h and 1, 7, and 14 days postseeding. Briefly, the specimens were harvested, washed twice with PBS (5 min per wash), and fixed with 3% glutaralde-hyde solution for 30 min. Then, the specimens were dehydrated in gradient ethanol (i.e., 30%, 50%, 70%, 80%, 90%, 95%, and 100%) and finally freeze dried. Subsequently, they were coated with gold and imaged via SEM.

Histological analysis

Histological analysis was performed at 4, 7, and 14 days postseeding. The collected specimens were rinsed twice with PBS (5 min per wash) and fixed in 10% neutral buffered formalin for 2 h; the specimens were then dehydrated and embedded in paraffin blocks. Longitudinal sections were stained with hematoxylin and eosin (H&E) to evaluate cell penetration.

Cell phenotypes imaged by LSCM

After 4, 7, and 14 days, the collected specimens were rinsed twice with PBS (5 min per wash), and then fixed with 4% paraformaldehyde for 20 min. Then, the TCs were permeabilized using 0.1% Triton X (Amresco). The cytoskeletons and nuclei of TCs were stained with 25 μg/mL rhodamine-labeled phalloidin (Biotium) and 10 μg/mL 4',6'-diamidino-2-phenylindole hydrochloride (DAPI; Beyotime), respectively. Subsequently, the specimens were visualized using laser scanning confocal microscopy (LSCM) (Carl Zeiss, LSM 510 META). Cell infiltration was further analyzed with imaging software that provided 3D views of the stained cells growing on the scaffolds.

Real-time polymerase chain reaction analysis

To determine the sensing and responding pattern of the TC on different scaffolds, the specific gene (type I collagen, type III collagen, decorin, tenascin-C, and biglycan) expressions of TCs were assessed using Real-time polymerase chain reaction (PCR) at 7 and 14 days. The TCs collected immediately before seeding served as controls. GAPDH and β-actin were used as housekeeping genes. Total RNA was extracted from TCs cultured on the scaffold samples with RNeasy Mini Kit (Qiagen). cDNA was transcribed reversely using an iScript™ cDNA synthesis kit (Bio-Rad). Real-time PCR was performed with a Power SYBR Green PCR Master Mix (Applied Biosystems) on a light cycle apparatus (Applied Biosystems 7500). All primer sequences were acquired from the literature[33,34] and designed with Primer 5.0 (Table 1). Three replicate analyses were performed for each specimen, and three PCR runs were performed for each gene. The level of target gene expression was calculated as $2^{-\triangle\triangle}Ct$.

Mechanical testing

Before and 14 days after cell seeding, the mechanical properties of the scaffold samples (length×width×thickness: $10\times10\times[0.1-0.15]$ mm) were evaluated using a uniaxial tester (Reger, RGT-5A) with a 1 MPa load cell. The cross-head speed was 10 mm/min. The tensile strength, Young's modulus, and elongation at break were calculated from the stress–strain curves ($n=3$).

Statistical analysis

All of the quantitative data are presented as the mean±standard deviation. One-way analysis of variance

TABLE 1. REAL-TIME POLYMERASE CHAIN REACTION PRIMERS USED IN THIS STUDY

Gene	GenBank ID	Sequence		Size
Type I collagen	D49399	Forward	5'CGCCTCTCAGAACATCACCTACC3'	121 bp
		Reverse	5'CTCGGCAACAAGTTCAACATCA 3'	
Type III collagen	S83371	Forward	5'GGCCCGCGTGGTGACAAAGG3'	177 bp
		Reverse	5'GGGGCCACTAGGTCCAACAGGT 3'	
Decorin	NM_001082330	Forward	5'TCCGCTGTCAGTGTCACCTTCG3'	99 bp
		Reverse	5'GCAGGTCCAGTAGCGTCGTGTC 3'	
Tenascin-C	XM_002720513	Forward	5'ATCACCACCAAGTTCACAACAG3'	143 bp
		Reverse	5'CCAATCCACAGATTCATAGAGCA3'	
Biglycan	NM_001195691	Forward	5'ATTGAGAACGGGAGCCTGAG3'	142 bp
		Reverse	5'CCTTGGTGATGTTGTTGGAAT3'	
β-actin	NW_003159504	Forward	5'TCTCTCGACGAAACCTAAC3'	141 bp
		Reverse	5'CCTTCACCGTTCCAGTTT3'	
GAPDH	L23961	Forward	5'GCCGCCTGGAGAAAGCTGCTAAG3'	157 bp
		Reverse	5'GCCCCAGCATCGAAGGTAGAGG 3'	

Primers for type I collagen, type III collagen, decorin, tenascin-C, biglycan, GAPDH, and β-actin were designed from Oryctolagus cuniculus gene sequences obtained from the NCBI GenBank and RefSeq databases using Primer 5.0 software.

was used to assess the statistical significance of results between groups. Differences were considered significant when $p < 0.05$.

Results

Scaffold morphology

The surface morphologies of the random nanofiber, aligned nanofiber, and nanoyarn scaffolds are shown in Figure 1 (A–F). Higher-magnification images revealed that the yarn in the nanoyarn scaffold was twisted by nanofibers (black arrow, Fig. 1F). The nanofibers in the aligned nanofiber scaffold and the yarns in the nanoyarn scaffold mainly formed angles ranging from 0° to 20° (Fig. 1H, I), while the nanofibers in the random nanofiber scaffold exhibited equal distribution at all angles (Fig. 1G). The nanofiber diameters of the three groups of scaffolds were comparable (632 ± 81 nm vs. 643 ± 97 nm vs. 641 ± 68 nm); however, the yarn diameter was significantly higher (9.51 ± 3.62 μm) in the nanoyarn scaffold (Fig. 1J). The nanoyarn scaffold exhibited a pore size (28.5 ± 17.42 μm) larger than the pore sizes of the random nanofiber (4.31 ± 1.95 μm) and aligned nanofiber (4.43 ± 2.16 μm) scaffolds (Fig. 1K).

Scaffold porosity

The nanoyarn scaffold exhibited a significantly increased porosity of $85.9\% \pm 8.3\%$ compared with the random nanofiber ($74.1\% \pm 1.3\%$) and aligned nanofiber scaffolds ($73.9\% \pm 2.5\%$) (Fig. 1L).

Fourier transform infrared spectroscopy

FTIR analysis revealed the compositions of the random nanofiber, aligned nanofiber, and nanoyarn scaffolds. As shown in Figure 2, there were two main absorption peaks at 1,653 and 1,552 cm^{-1} in pure collagen, corresponding to amide I and amide II,[35] respectively. Two representative absorption peaks at 1,756 and 1,735 cm^{-1}, corresponding to C-O stretching in poly(L-lactide) and poly(ε-caprolactone), respectively, were detected in the P(LLA-CL) FTIR spectra. The same absorption peaks were observed in the nanofiber and nanoyarn scaffolds

spectra, indicating the presence of collagen in the final random nanofiber, aligned nanofiber, and nanoyarn scaffolds.

Cell adhesion and proliferation

According to the results obtained by the CCK-8 assay (Fig. 3). Initial cell adhesion is reflected by the counted cell number 4 h postseeding. No significant differences in the number of adhered cells were observed between the groups during the first 4 h, although the number of adhered cells was slightly higher on the nanoyarn scaffold than that on the other scaffolds. Cell proliferation studies were performed at 1, 7, and 14 days. There were no significant differences in the number of cells between the groups after 1 day culture. However, cell proliferation on the nanoyarn scaffold was significantly higher than that on the random nanofiber scaffold, aligned nanofiber scaffold, and the TCPS controls at 4, 7, and 14 days.

Cell morphologies on the scaffolds imaged by SEM

SEM images depicting cell adhesion and morphology are presented in Figures. 4 and 5, respectively. As shown in Figure 4, 4 h after seeding, the TCs on the three groups of substrates appeared to have a round shape (Fig. 4A–C). Higher-magnification images (Fig. 4D–F) revealed that the TCs had extended their cytoplasm in the form of thin and long fibrils from the leading edges (arrows), similar to lamellipodia; these fibrils suggested that the TCs could fully attach to the nanoyarn and nanofiber substrates. In addition, the TCs could attach to the large pores of the nanoyarn scaffold (Fig. 4C), unlike those on the random nanofiber and aligned nanofiber scaffolds (Fig. 4A, B).

By day 1, TCs were well spread on the random nanofiber scaffold, exhibiting polygonal shapes and random orientations (Fig. 5A). However, the TCs seeded on the aligned nanofiber and nanoyarn scaffolds exhibited a spindle-shaped morphology and spread along with substrate fibers (Fig. 5B, C, arrow); in addition, some cells were located inside the pores of nanoyarn scaffolds (Fig. 5C). By day 7, all cell-seeded scaffolds were apparently filled with cell sheets and possibly ECM secreted by the TCs (Fig. 5D–F). After 14 days of culture, all cell-seeded scaffolds were completely filled with seemingly
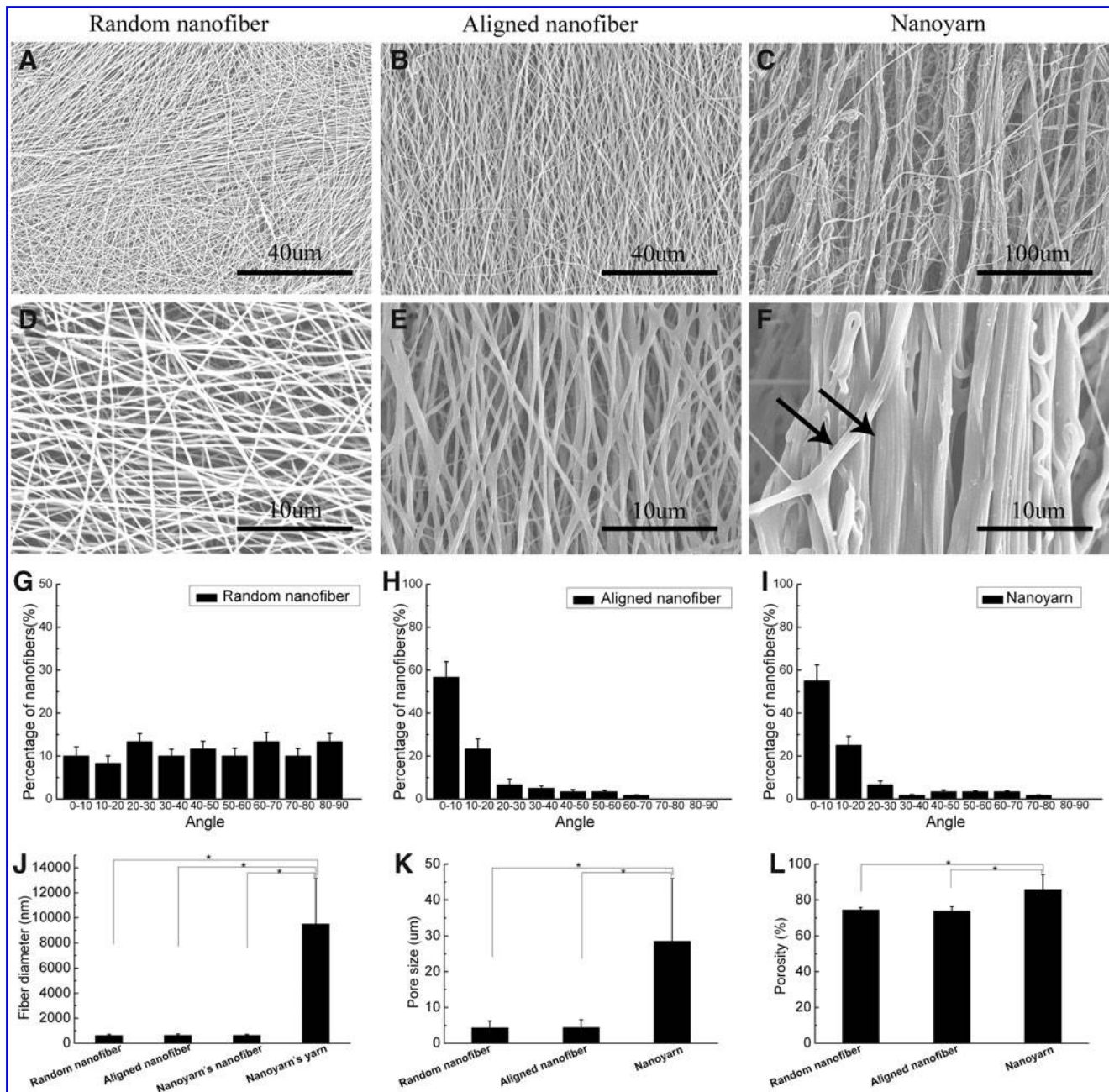
FIG. 1. Scanning electron microscopy (SEM) micrographs of electrospun poly(l-lactide-co-ε-caprolactone) [P(LLA-CL)]/ collagen with random nanofiber **(A, D)**, aligned nanofiber **(B, E)**, and nanoyarn **(C, F)** scaffold surface morphology. Images **(D–F)** are higher magnification images of **(A–C)**; the arrow in **(F)** indicates the yarn was twisted by nanofibers in the nanoyarn scaffold (scale bars: 40 μm for **A** and **B**; 100 μm for **C**; and 10 μm for **D, E,** and **F**). **(G–I)** Histograms representing the angular distributions of the nanofibers in the random nanofiber and aligned nanofiber scaffolds and the yarns in the nanoyarn scaffold, respectively. **(J)** Histogram representing the fiber diameter of the nanofibers in the three scaffolds and the yarns in the nanoyarn scaffold. **(K)** Histogram representing the pore size of the three scaffolds. **(L)** Histogram representing the porosity of the three scaffolds. The data are expressed as the mean ± standard deviation (SD). The samples indicated with (*) had a significant difference between the two groups ($p < 0.05$).

thick cell sheets and ECM (Fig. 5G–I). The original structural outline of the scaffold samples could not be detected.

Histological analysis

Magnified H&E-stained images of the scaffold samples section are presented in Figure 6. Infiltration of TCs from the top surface to the bottom was observed. By day 4, the TCs had infiltrated to a depth of ∼40 μm (yellow arrow) from the surface (Fig. 6C). After 7 (Fig. 6F) and 14 (Fig. 6I) days of culture, the cells had infiltrated nearly the entire scaffold (yellow arrow), suggesting that the growing cells had attached to and infiltrated the porous skeleton of the nanoyarn scaffold. In contrast, cellular activities in the random
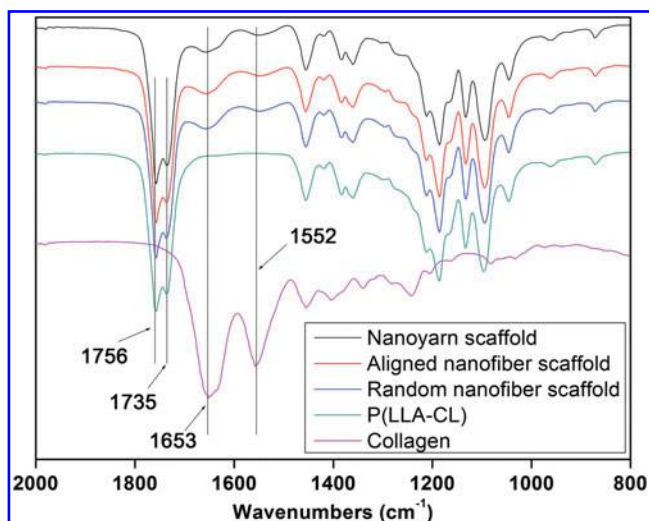
FIG. 2. Fourier transform infrared spectroscopy spectra of the collagen, P(LLA-CL), and P(LLA-CL)/collagen with the random nanofiber, aligned nanofiber, and nanoyarn scaffolds. Showing the presence of collagen and P(LLA-CL) in the newly designed scaffold. Color images available online at www.liebertpub.com/tec

nanofiber (Fig. 6A, D, G) and aligned (Fig. 6B, E, H) nanofiber scaffolds were mainly confined to the dense upper layer (green arrow).

Cell phenotypes imaged by LSCM

TCs grown on the scaffold samples were stained with rhodamine-labeled phalloidin and DAPI. A series of confocal sections were acquired from the top surface to a depth of $100 \mu m$ along the z-axis with a LSCM. The 3D structure of the
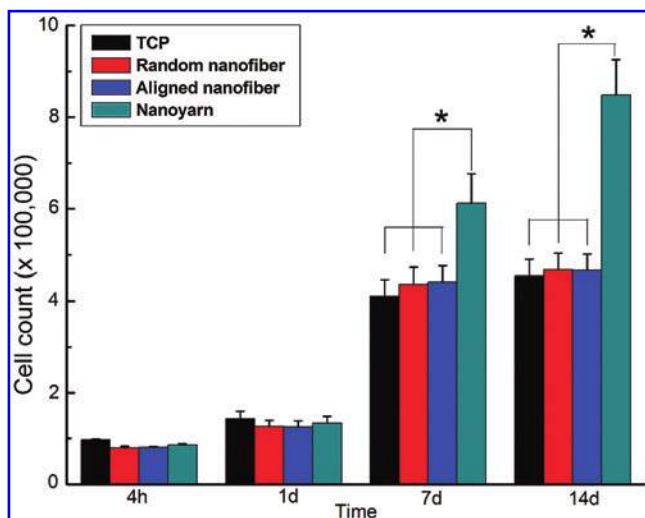

FIG. 3. CCK-8 result of tendon cells (TCs) cultured on tissue-culture polystyrene plate (TCPS), P(LLA-CL)/collagen random nanofiber, aligned nanofiber, and nanoyarn scaffolds for 4 h, 1, 7, and 14 days. The data are expressed as the mean ± SD. The samples indicated with (*) had a significant difference between the two groups ($p < 0.05$). Color images available online at www.liebertpub.com/tec

growth of the TCs within the scaffold was elucidated by imaging stained cells with Image software. From the horizontal view, after 4 days of culture, TCs spreading on the aligned nanofiber (Fig. 7B, green arrow) and nanoyarn scaffolds (Fig. 7C, green arrow) were visible with aligned actin filaments, whereas TCs spreading on the random nanofiber scaffold were visible with unaligned actin filaments (Fig. 7A). More cell nuclei and actin bundles were observed on the three scaffolds after 7 (Fig. 7D–F) and 14 (Fig. 7G–I) days. From the sagittal view, the 3D CLSM images of TCs on the nanoyarn scaffold clearly demonstrated that the cytoskeletons of TCs appeared ~40 μm from the surface (yellow arrow) after 4 days of culture (Fig. 7c), as calculated using Image software, ~70 μm (yellow arrow) from the surface after 7 days (Fig. 7f) and nearly 90 μm (yellow arrow) from the surface after 14 days (Fig. 7i). This phenomenon implies that after a certain period of culture, TCs could infiltrate the entire porous skeleton of the nanoyarn scaffold. However, the cytoskeletons of TCs only appeared on the surfaces of the random nanofiber (Fig. 7a, d, g) and aligned nanofiber (Fig. 7b, e, h) scaffolds at 4, 7, and 14 days.

Phenotypical expression of tendon-related ECM genes

Real-time PCR revealed differences in the tendon-related ECM genes expression profiles for TCs cultured on the different scaffolds (Fig. 8). By day 7, the expression levels of type I collagen, decorin, tenascin-C, and biglycan were significantly elevated on the nanoyarn scaffold compared with the random nanofiber scaffold, and the expression levels of type I collagen, tenascin-C, and biglycan were significantly elevated on the aligned scaffold compared with the random nanofiber scaffold. However, the expression levels of the five tendon-specific ECM genes were not significantly different between nanoyarn scaffold and aligned nanofiber scaffold. By day 14, the expression levels of the five tendon-specific ECM genes within the nanoyarn scaffold were significantly upregulated compared with the random nanofiber and aligned nanofiber scaffolds. However, the expression levels of the five tendon-specific ECM genes were not significantly different between random nanofiber scaffold and aligned nanofiber scaffold.

Mechanical testing

The tensile properties of the scaffold samples are presented in Figure 9. Before cell seeding, the nanoyarn scaffold had a lower Young's modulus and lower tensile strength, but higher elongation at break compared with random nanofiber and aligned nanofiber scaffolds. After 14 days of cell seeding, both the Young's modulus and tensile strength of the cell-seeded nanoyarn scaffold were significantly elevated compared with the unseeded nanoyarn scaffold, and these two values of cell-seeded random nanofiber and aligned nanofiber scaffolds also increased compared with the unseeded random nanofiber and aligned nanofiber scaffolds, respectively; although the differences were not significantly different.

Discussion

Despite widespread investigation and considerable progress, there have been few products available for clinical applications in tendon tissue engineering over the past two decades. One key reason for this scarcity is that scaffolds
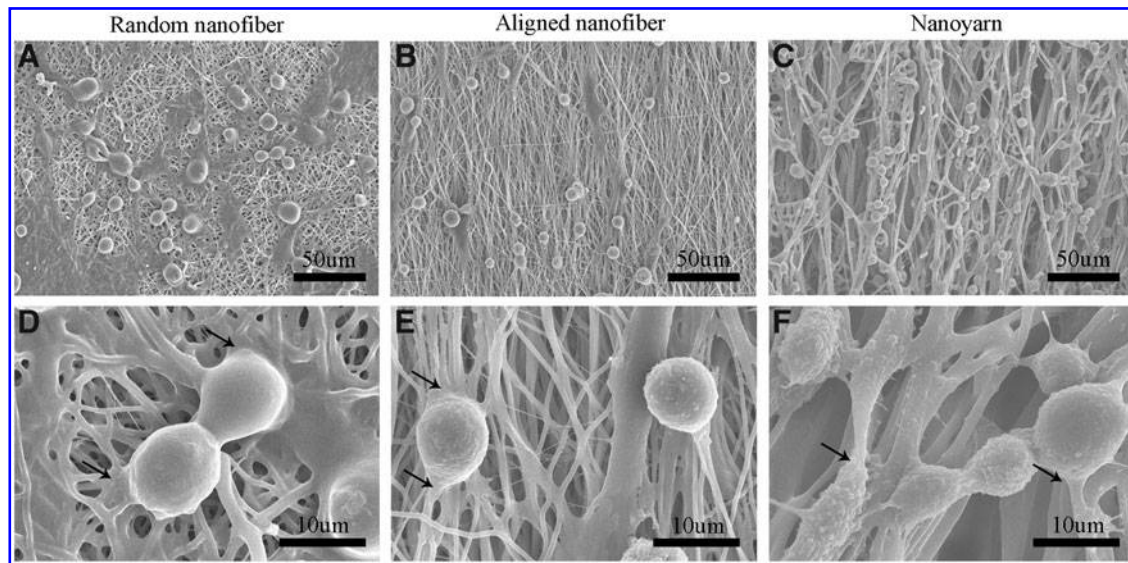
FIG. 4. SEM observations of TCs cultured on P(LLA-CL)/collagen random nanofiber **(A, D)**, aligned nanofiber **(B, E)**, and nanoyarn **(C, F)** scaffolds for 4 h. Images **(D–F)** are higher magnification images of **(A–C)**; the thin and long fibrils (arrow) of TCs were observed in **(D–F)** (scale bars: 50 μm for **A, B,** and **C**; 10 μm for **D, E,** and **F**).

with desirable properties are still under development. We used a novel electrospun fiber manipulation process to fabricate a P(LLA-CL)/collagen nanoyarn scaffold with a 3D, porous, aligned microstructure that morphologically and structurally mimics native tendon. The 3D macropores, together with the aligned properties, provide a satisfactory biological environment for TC growth.

Tendons/ligaments rely on a highly organized microstructure to impart their desired functionality.[1] As shown in Figure 1, the P(LLA-CL)/collagen random nanofiber, aligned nanofiber, and nanoyarn scaffolds exhibited similar nanoscale fiber diameters, and the yarn in the nanoyarn scaffolds was twisted by many nanofibers, causing an increased

diameter (Fig. 1J). The nanoyarn scaffold also exhibited highly aligned structures similar to the aligned nanofiber scaffold (Fig. 1H, I). The majority of aligned yarns in the nanoyarn scaffold were similar in structure and inherent nanoscale organization to tendons, while the other cross-linking yarns in the nanoyarn scaffold were able to form 3D macropores (Fig. 1C). Additionally, the nanoyarn scaffold exhibited a larger pore size and higher porosity than the random nanofiber and aligned nanofiber scaffolds (Fig. 1K, L). Porosity is the fundamental characteristic that enables scaffolds to provide space for cell adhesion and migration, allowing for nutrition transport and metabolite discharge.[36,37]
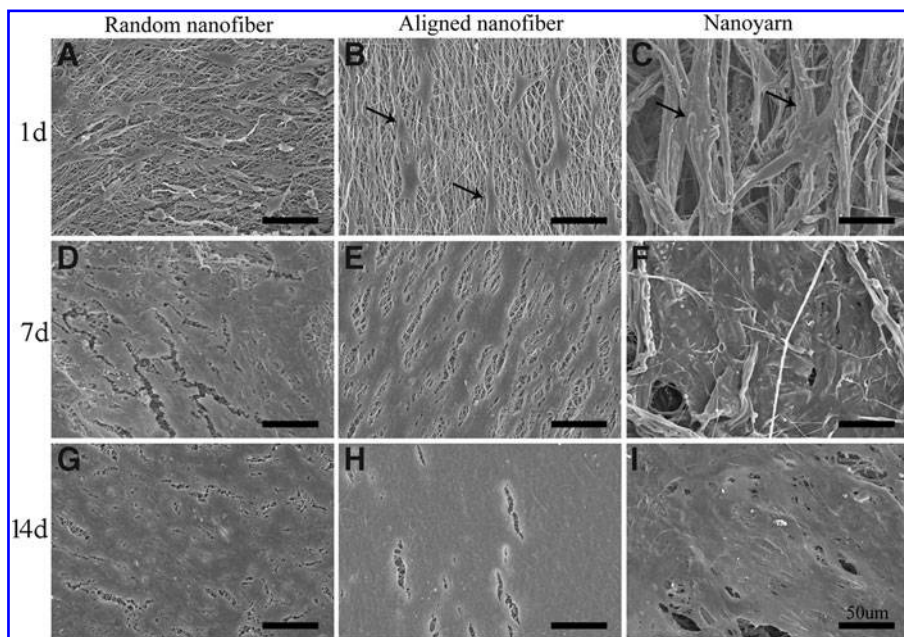

FIG. 5. SEM observations of TCs cultured on P(LLA-CL)/collagen random nanofiber **(A, D, G)**, aligned nanofiber **(B, E, H)**, and nanoyarn **(C, F, I)** scaffolds for 4, 7, and 14 days, respectively. Spindle-shaped TCs (arrow) along the direction of fibers were observed in **(B)** and **(C)**. The scale on all images = 50 μm.

FIG. 6. Images of H&E-stained sections of P(LLA-CL)/collagen random nanofiber and aligned nanofiber scaffolds seeded with TCs after 4 **(A, B)**, 7 **(D, E)**, and 14 **(G, H)** days of culture show that cellular infiltration is limited to the top layers of the scaffolds (green arrow). Images of H&E-stained sections of P(LLA-CL)/collagen nanoyarn scaffolds after 4 **(C)**, 7 **(F)**, and 14 **(I)** days of culture show that there is a progressive infiltration and growth of cells into the scaffolds (yellow arrow) throughout the 14 days. The scale on all images = 100 μm. Color images available online at www.liebertpub.com/tec
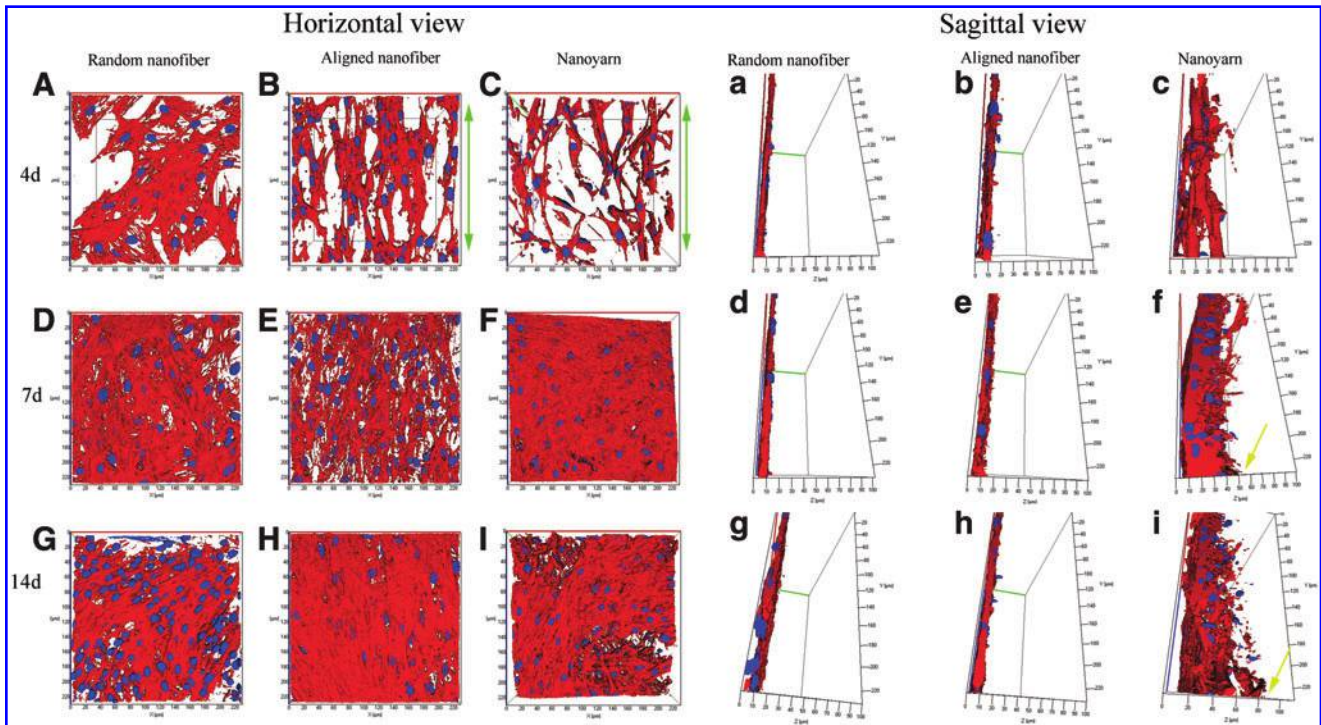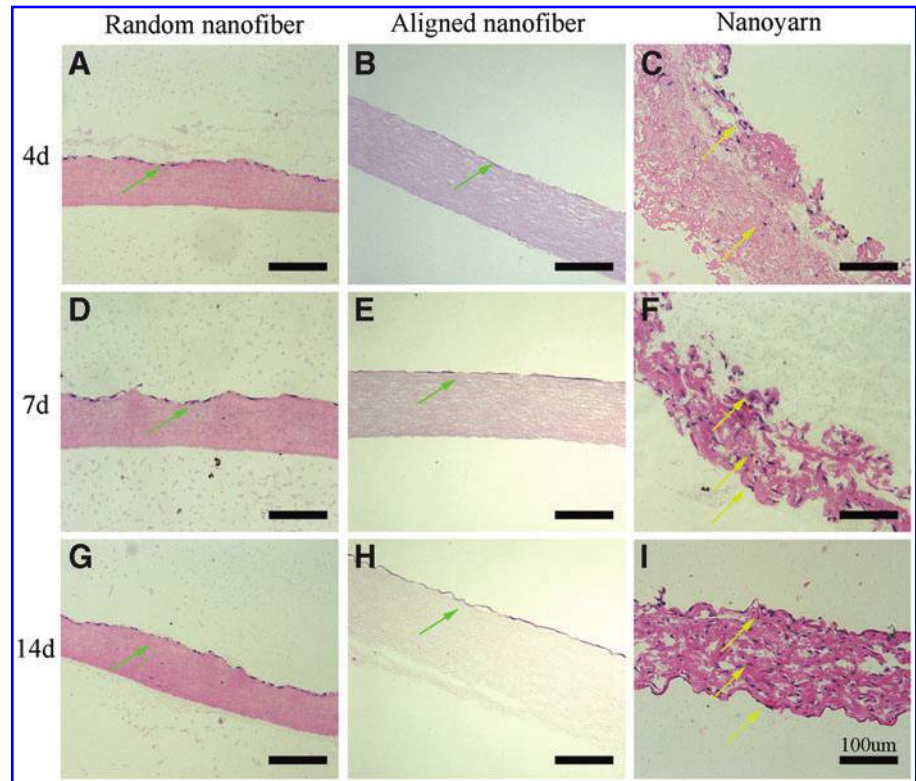

FIG. 7. Confocal microscopy reconstructed stacks of three-dimensional fluorescence images of the cytoplasm (red) and nuclei (blue) of TCs on P(LLA-CL)/collagen random nanofiber **(A, D, G)**, aligned nanofiber **(B, E, H)**, and nanoyarn **(C, F, I)** scaffolds after 4, 7, and 14 days of culture, respectively. The aligned actin filaments of TCs (green arrow) along the direction of fibers were observed in **(B)** and **(C)**. Images **a–i** are the sagittal views of **A–I** (horizontal view). The cytoskeletons of TCs in **(c)**, **(f)**, and **(i)** show a progressive infiltration and growth into the nanoyarn scaffolds (yellow arrow) throughout the 14 days of culture. All images are 200 × 200 × 100 μm. Color images available online at www.liebertpub.com/tec
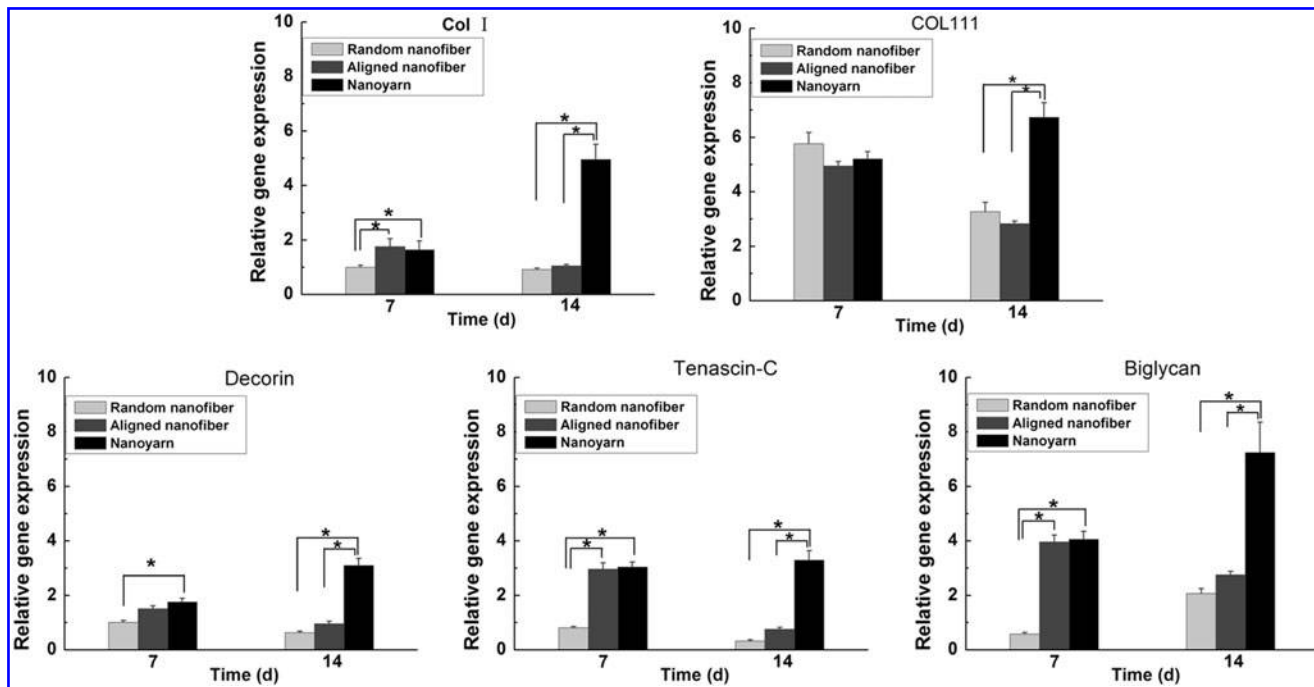
FIG. 8. The expressions of type I collagen, type III collagen, decorin, tenascin-C, and biglycan in TCs cultured on P(LLA-CL)/collagen random nanofiber, aligned nanofiber, and nanoyarn scaffolds for 7 and 14 days. The expression levels, quantified using real-time PCR, are normalized to those of housekeeping genes, GADPH and β-actin. TCs obtained immediately prior to seeding on scaffolds served as controls (the values of the expressions of tendon extracellular matrix genes are treated as 1 in this group). The data are expressed as the mean±SD. The samples indicated with (*) had a significant difference between the two groups ($p < 0.05$), ($n = 3$).

In the present study, FTIR analysis (Fig. 2) demonstrated that collagen was present in all of the random nanofiber, aligned nanofiber, and nanoyarn scaffolds. Composite synthetic and natural polymer scaffolds contain functional groups, such as amino, hydroxyl, and carboxyl groups, that can improve their hydrophilicity and biocompatibility.[38,39]

TCs derived from the tendons of adult Oryctolagus cuniculus in this study were seeded on P(LLA-CL)/collagen random nanofiber, aligned nanofiber, and nanoyarn scaffolds. According to the results obtained by the CCK-8 assay (Fig. 3) and SEM (Figs. 4, 5), the three scaffolds have no negative effects on TC adhesion or proliferation *in vitro*. These results also suggest that the nanoyarn scaffold can provide a better structure for cell proliferation than the random nanofiber scaffold, aligned nanofiber scaffold, and TCPS controls, which may be due to its large pore size and

higher porosity. A previous literature[40] reported that a P(LLA-CL)/collagen nanofiber scaffold could support cell proliferation and promote tissue regeneration. Cells are highly sensitive to nanofiber structure, fiber diameter, and orientation. These three factors affect the differentiation and function of cells.[30] Our results indicate that TCs spread along the fibers in the aligned nanofiber and nanoyarn scaffolds and exhibited a typical spindle-shaped morphology (Fig. 5B, C). TCs spreading on the aligned nanofiber and nanoyarn scaffolds were visible with aligned actin filaments (Fig. 7B, C), which suggests that the TCs sense substrates topography, transform such information into morphological changes, and exhibited native morphology on the aligned nanofiber and nanoyarn scaffolds.[41] Contact guidance theories help explain the relationship between cell morphology and fiber arrangement. A substrate with appropriate topographical
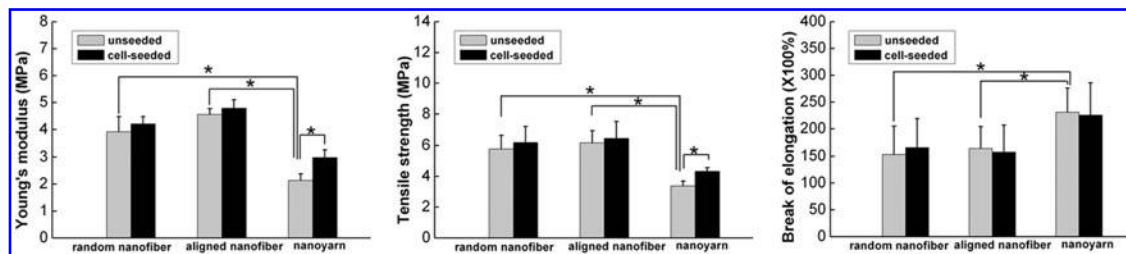

FIG. 9. The Young's modulus, tensile strength, and elongation at the break of P(LLA-CL)/collagen random nanofiber, aligned nanofiber, and nanoyarn scaffolds before cell seeding and after 14 days of cell culture. Data are expressed as means±SD. Samples indicated with (*) had a significant difference between two groups ($p < 0.05$), ($n = 3$).

features could guide the arrangement and migration of cells via adhesion-cytoskeleton interactions.[42]

A successful tissue-engineered scaffold should not only facilitate cell attachment and proliferation but should also support cell infiltration and ultimately promote the formation of the entire tissues. According to the results of our histological assessment (Fig. 6) and the 3D images (Fig. 7) obtained by confocal microscopy, the nanoyarn scaffold offered a 3D and adequately porous structure for cell infiltration and growth. Additionally, the interspaces of the scaffold were observed to be fully filled with the ECM secreted by TCs. However, there was only one cell sheet that formed on the surface of random nanofiber and aligned nanofiber scaffolds. One key factor that affects the application of tissue-engineered electrospun nanofiber scaffolds is that cells can hardly infiltrate the 3D structure of the scaffolds.[43] An ideal tissue-engineered scaffold should have at least 70% porosity[44] and pore sizes ranging from tens to hundreds of microns[45] to provide a suitable 3D space. Thus, compared with the random nanofiber and aligned nanofiber scaffolds, the nanoyarn scaffold provides sufficient space for cell adhesion and infiltration.

The phenotypic expression of tendon-related ECM genes was quantitatively determined via real-time PCR (Fig. 8). Type I and type III collagen are the primary matrix components of native tendons/ligaments.[27] Decorin is a primary proteoglycan that affects collagen fiber diameter and maturity in tendons.[3] Tenascin-C is an early marker in embryonic tendon.[46] Biglycan is also a primary proteoglycan and contributes to thick collagen fibrillogenesis and collagen fibril organization.[47] The phenotypic expression levels of tendon-specific ECM genes of TCs on the nanoyarn and aligned nanofiber scaffolds were higher than those on the random nanofiber scaffold on day 7, which suggests that contact guidance cues from the aligned architecture of the nanoyarn and aligned nanofiber substrates can stimulate higher expression of the tendon-specific ECM genes of the TCs. Interphase nucleus organization and genomic regulation may be affected by morphological changes induced in cytoskeleton by substrates[42]. By day 14, the phenotypic expression levels of tendon-related ECM genes of TCs on the nanoyarn scaffold were higher than those on the random nanofiber and aligned nanofiber scaffolds, which is explained by the nanoyarn scaffold's high porosity and large pores. Caliari et al. demonstrated that a scaffold with a larger pore size supported higher TC metabolic activity due to its higher permeability.[48] These results suggest that the nanoyarn scaffold effectively improves the bioactivity and expression of tendon-related ECM genes of TCs.

A major challenge developing tensile stress-bearing scaffolds for tendon tissue engineering lies in balancing the porosity and mechanical properties of these scaffolds.[49] High porosity promotes cell growth, proliferation, nutrient exchange, and waste discharge; however, these advantages are afforded at the cost of reduced mechanical strength. No definitive standard has been established yet for the appropriate relationship between these two factors in tendon tissue engineering. Before implantation, tendon tissue engineering constructs often undergo a certain period of in vitro cultivation under mechanically static culture conditions.[50] Human ligaments and tendons have a maximum strength ranging from 4.4 to 660 MPa and a maximum strain of 18%–30%.[51,52] The elastic moduli observed for adult human ligaments and tendons are 0.2–1.5 GPa.[53,54] Our studies (Fig. 9) demonstrated that nanoyarn scaffolds exhibit a tensile strength that is nearly half of the minimum strength of native ligaments, which enables them to provide sufficient mechanical support for functional exercise after implantation in vivo. Additionally, the nanoyarn scaffold developed in this study has sufficient elasticity to avoid prolongation and fragmentation under biomechanical stimulation. Undeniably, nanoyarn scaffolds exhibit lower tensile strength and Young's modulus values than do human ligaments and tendons. Although these scaffolds failed to precisely match the stiffness, flexibility, and viscoelasticity of native tendons, we expected that the biochemical and mechanical properties of native tendons were approximately imitated by combining the nanoyarn scaffolds with TCs to promoting ECM remodeling. After 14 days of cell seeding, all three types of scaffolds exhibited an increased Young's modulus and tensile strength. This result suggests that the overall strength of the scaffolds may be increased by the ECM that is secreted onto the fibers by the seeded cells, which is consistent with the results of a previous study.[55] Only in the nanoyarn group were the Young's modulus and tensile strength of the cell-seeded scaffold significantly elevated than those of the unseeded scaffold, which may suggest that the nanoyarn scaffold has an appropriate 3D porous architecture to support more cell ingrowth. Thus, having more ECM deposited by cells in the nanoyarn scaffold is meaningful in the resulting increased modulus and tensile strength.

In a future study, we will culture cell-scaffold constructs in a bioreactor under dynamic loading conditions to promote the deposition of ECM over the entire scaffolds, which can in turn increase the mechanical support. The mechanical strength of the scaffolds must be further evaluated after the cell-scaffold constructs are transplanted in vivo. The biodegradation of the scaffolds was not evaluated in this study and will be examined in the future.

Conclusions

A tendon tissue engineering scaffold, P(LLA-CL)/collagen nanoyarn network, that mimics the ECM of native tendon in terms of structure and inherent nanoscale organization, has been fabricated using a novel electrospinning technology. The P(LLA-CL)/collagen nanoyarn scaffold has a 3D aligned microstructure, larger pore size, and higher porosity compared with P(LLA-CL)/collagen random nanofiber and aligned nanofiber scaffolds. TCs exhibited native morphology and improved cellular proliferation on the nanoyarn scaffold compared with cells cultured on the random nanofiber and aligned nanofiber scaffolds. Moreover, the spatial structure of the nanoyarn scaffold is beneficial for cell infiltration. In addition, this scaffold exhibits desirable mechanical properties for tendon tissue regeneration. This study demonstrates that electrospun P(LLA-CL)/collagen nanoyarn is a novel, 3D, macroporous, aligned scaffold that satisfies the requirements for functional tendon tissue engineering.

Acknowledgments

Disclosure Statement

No competing financial interests exist.

References

1. Wang, J.H.C. Mechanobiology of tendon. J Biomech **39,** 1563, 2006.
2. Sahoo, S., Ouyang, H., Goh, J.C.H., Tay, T., and Toh, S. Characterization of a novel polymeric scaffold for potential application in tendon/ligament tissue engineering. Tissue Eng **12,** 91, 2006.
3. Chen, J.L., Yin, Z., Shen, W.L., Chen, X., Heng, B.C., Zou, X.H., and Ouyang, H.W. Efficacy of hESC-MSCs in knitted silk-collagen scaffold for tendon tissue engineering and their roles. Biomaterials **31,** 9438, 2010.
4. Ma, P.X. Biomimetic materials for tissue engineering. Adv Drug Deliv Rev **60,** 184, 2008.
5. Omae, H., Zhao, C., Sun, Y.L., An, K.N., and Amadio, P.C. Multilayer tendon slices seeded with bone marrow stromal cells: a novel composite for tendon engineering. J Orthop Res **27,** 937, 2009.
6. Franco, B., Vincenzo, V., Alessandro, D.V., Tonello, C., Abatangelo, G., and Mazzoleni, F. Tissue engineering approaches for the construction of a completely autologous tendon substitute. Indian J Plast Surg **41,** 38, 2008.
7. Juncosa-Melvin, N., Shearn, J.T., Boivin, G.P., Gooch, C., Galloway, M.T., West, J.R., Nirmalanandhan, V.S., Bradica, G., and Butler, D.L. Effects of mechanical stimulation on the biomechanics and histology of stem cell-collagen sponge constructs for rabbit patellar tendon repair. Tissue Eng **12,** 2291, 2006.
8. Bagnaninchi, P., Yang, Y., Zghoul, N., Maffulli, N., Wang, R., and Haj, A.J.E. Chitosan microchannel scaffolds for tendon tissue engineering characterized using optical coherence tomography. Tissue Eng **13,** 323, 2007.
9. Goh, J., and Toh, S. Novel silk scaffold/cell-sheet system for ligament and tendon tissue engineering. J Biomech **39,** S60, 2006.
10. Guo, Z., Chen, J.J., and Zhang, P.H. A knitted scaffold for tendon engineering using poly (lactic acid) fibers. Adv Mater Res **197,** 164, 2011.
11. Ouyang, H.W., Goh, J.C.H., Thambyah, A., Teoh, S.H., and Lee, E.H. Knitted poly-lactide-co-glycolide scaffold loaded with bone marrow stromal cells in repair and regeneration of rabbit Achilles tendon. Tissue Eng **9,** 431, 2003.
12. Liu, W., Chen, B., Deng, D., Xu, F., Cui, L., and Cao, Y. Repair of tendon defect with dermal fibroblast engineered tendon in a porcine model. Tissue Eng **12,** 775, 2006.
13. Zhang, X., Bogdanowicz, D., Erisken, C., Lee, N.M., and Lu, H.H. Biomimetic scaffold design for functional and integrative tendon repair. J Shoulder Elbow Surg **21,** 266, 2012.
14. Sill, T.J., and von Recum, H.A. Electrospinning: applications in drug delivery and tissue engineering. Biomaterials **29,** 1989, 2008.
15. Zhou, J., Cao, C., Ma, X., and Lin, J. Electrospinning of silk fibroin and collagen for vascular tissue engineering. Int J Biol Macromol **47,** 514, 2010.
16. Mukherjee, S., Gualandi, C., Focarete, M.L., Ravichandran, R., Venugopal, J.R., Raghunath, M., and Ramakrishna, S. Elastomeric electrospun scaffolds of poly(L-lactide-co-trimethylene carbonate) for myocardial tissue engineering. J Mater Sci Mater Med **22,** 1689, 2011.
17. McCullen, S.D., Miller, P.R., Gittard, S.D., Gorga, R.E., Pourdeyhimi, B., Narayan, R.J., and Loboa, E.G. *In situ* collagen polymerization of layered cell-seeded electrospun scaffolds for bone tissue engineering applications. Tissue Eng Part C Methods **16,** 1095, 2010.
18. Yang, Y., Zhu, X., Cui, W., Li, X., and Jin, Y. Electrospun composite mats of poly [(D, L-lactide)-co-glycolide] and collagen with high porosity as potential scaffolds for skin tissue engineering. Macromol Mater Eng **294,** 611, 2009.
19. Subramanian, A., Vu, D., Larsen, G.F., and Lin, H.Y. Preparation and evaluation of the electrospun chitosan/PEO fibers for potential applications in cartilage tissue engineering. J Biomater Sci Polym Ed **16,** 861, 2005.
20. Vaquette, C., Kahn, C., Frochot, C., Nouvel, C., Six, J.L., De Isla, N., Luo, L.H., Cooper-White, J., Rahouadj, R., and Wang, X. Aligned poly (L-lactic-co-e-caprolactone) electrospun microfibers and knitted structure: a novel composite scaffold for ligament tissue engineering. J Biomed Mater Res Part A **94,** 1270, 2010.
21. Lee, J., Guarino, V., Gloria, A., Ambrosio, L., Tae, G., Kim, Y.H., Jung, Y., and Kim, S.H. Regeneration of Achilles' tendon: the role of dynamic stimulation for enhanced cell proliferation and mechanical properties. J Biomater Sci Polym Ed **21,** 1173, 2010.
22. Xu, C., Inai, R., Kotaki, M., and Ramakrishna, S. Electrospun nanofiber fabrication as synthetic extracellular matrix and its potential for vascular tissue engineering. Tissue Eng **10,** 1160, 2004.
23. Xie, J., Ihara, M., Jung, Y., Kwon, I.K., Kim, S.H., Kim, Y.H., and Matsuda, T. Mechano-active scaffold design based on microporous poly (L-lactide-co-ε-caprolactone) for articular cartilage tissue engineering: dependence of porosity on compression force-applied mechanical behaviors. Tissue Eng **12,** 449, 2006.
24. Keun Kwon, I., Kidoaki, S., and Matsuda, T. Electrospun nano-to microfiber fabrics made of biodegradable copolyesters: structural characteristics, mechanical properties and cell adhesion potential. Biomaterials **26,** 3929, 2005.
25. Fang, Z., Fu, W., Dong, Z., Zhang, X., Gao, B., Guo, D., He, H., and Wang, Y. Preparation and biocompatibility of electrospun poly (l-lactide-co-ε-caprolactone)/fibrinogen blended nanofibrous scaffolds. Appl Surface Sci **257,** 4133, 2011.
26. Harley, B.A.C., and Gibson, L.J. *In vivo* and *in vitro* applications of collagen-GAG scaffolds. Chem Eng J **137,** 102, 2008.
27. Liu, H., Fan, H., Toh, S.L., and Goh, J.C.H. A comparison of rabbit mesenchymal stem cells and anterior cruciate ligament fibroblasts responses on combined silk scaffolds. Biomaterials **29,** 1443, 2008.
28. Kuo, C.K., Marturano, J.E., and Tuan, R.S. Novel strategies in tendon and ligament tissue engineering: advanced biomaterials and regeneration motifs. Sports Med Arthrosc Rehabil Ther Tech SMARTT **2,** 20, 2010.
29. Blakeney, B.A., Tambralli, A., Anderson, J.M., Andukuri, A., Lim, D.J., Dean, D.R., and Jun, H.W. Cell infiltration and growth in a low density, uncompressed three-dimensional electrospun nanofibrous scaffold. Biomaterials **32,** 1583, 2011.
30. Beachley, V., and Wen, X. Polymer nanofibrous structures: fabrication, biofunctionalization, and cell interactions. Prog Polym Sci **35,** 868, 2010.
31. Teo, W.E., Gopal, R., Ramaseshan, R., Fujihara, K., and Ramakrishna, S. A dynamic liquid support system for continuous electrospun yarn fabrication. Polymer **48,** 3400, 2007.
32. Teo, W., Liao, S., Chan, C., and Ramakrishna, S. Remodeling of three-dimensional hierarchically organized nanofibrous assemblies. Curr Nanosci **4,** 361, 2008.

33. Sahoo, S., Toh, S.L., and Goh, J.C.H. A bFGF-releasing silk/PLGA-based biohybrid scaffold for ligament/tendon tissue engineering using mesenchymal progenitor cells. Biomaterials **31,** 2990, 2010.

34. Sawaguchi, N., Majima, T., Funakoshi, T., Shimode, K., Harada, K., Minami, A., and Nishimura, S.I. Effect of cyclic three-dimensional strain on cell proliferation and collagen synthesis of fibroblast-seeded chitosan-hyaluronan hybrid polymer fiber. J Orthop Sci **15,** 569, 2010.

35. Park, S.N., Park, J.C., Kim, H.O., Song, M.J., and Suh, H. Characterization of porous collagen/hyaluronic acid scaffold modified by 1-ethyl-3-(3-dimethylaminopropyl) carbodiimide cross-linking. Biomaterials **23,** 1205, 2002.

36. Agrawal, C., and Ray, R.B. Biodegradable polymeric scaffolds for musculoskeletal tissue engineering. J Biomed Mater Res **55,** 141, 2001.

37. Zeltinger, J., Sherwood, J.K., Graham, D.A., Müeller, R., and Griffith, L.G. Effect of pore size and void fraction on cellular adhesion, proliferation, and matrix deposition. Tissue Eng **7,** 557, 2001.

38. Chandrasekaran, A.R., Venugopal, J., Sundarrajan, S., and Ramakrishna, S. Fabrication of a nanofibrous scaffold with improved bioactivity for culture of human dermal fibroblasts for skin regeneration. Biomed Mater **6,** 015001, 2011.

39. Kwon, I.K., and Matsuda, T. Co-electrospun nanofiber fabrics of poly (L-lactide-co-ε-caprolactone) with type I collagen or heparin. Biomacromolecules **6,** 2096, 2005.

40. Prabhakaran, M.P., Sreekumaran Nair, A., Kai, D., and Ramakrishna, S. Electrospun composite scaffolds containing poly (octanediolco-citrate) for cardiac tissue engineering. Biopolymers **97,** 529, 2012.

41. Chen, C.S., Mrksich, M., Huang, S., Whitesides, G.M., and Ingber, D.E. Geometric control of cell life and death. Science **276,** 1425, 1997.

42. Chew, S.Y., Mi, R., Hoke, A., and Leong, K.W. The effect of the alignment of electrospun fibrous scaffolds on Schwann cell maturation. Biomaterials **29,** 653, 2008.

43. Zhong, S., Zhang, Y., and Lim, C.T. Fabrication of large pores in electrospun nanofibrous scaffolds for cellular infiltration: a review. Tissue Eng Part B Rev **18,** 77, 2012.

44. Ma, P.X. Scaffolds for tissue fabrication. Mater Today **7,** 30, 2004.

45. Oh, S.H., Park, I.K., Kim, J.M., and Lee, J.H. *In vitro* and *in vivo* characteristics of PCL scaffolds with pore size gradient fabricated by a centrifugation method. Biomaterials **28,** 1664, 2007.

46. Amiel, D., Frank, C., Harwood, F., Fronek, J., and Akeson, W. Tendons and ligaments: a morphological and biochemical comparison. J Orthop Res **1,** 257, 2005.

47. Tremble, P., Chiquet-Ehrismann, R., and Werb, Z. The extracellular matrix ligands fibronectin and tenascin collaborate in regulating collagenase gene expression in fibroblasts. Mol Biol Cell **5,** 439, 1994.

48. Caliari, S.R., and Harley, B.A. The effect of anisotropic collagen-GAG scaffolds and growth factor supplementation on tendon cell recruitment, alignment, and metabolic activity. Biomaterials **32,** 5330, 2011.

49. Ramay, H.R.R., and Zhang, M. Biphasic calcium phosphate nanocomposite porous scaffolds for load-bearing bone tissue engineering. Biomaterials **25,** 5171, 2004.

50. Liu, Y., Ramanath, H.S., and Wang, D.A. Tendon tissue engineering using scaffold enhancing strategies. Trends Biotechnol **26,** 201, 2008.

51. De Santis, R., Sarracino, F., Mollica, F., Netti, P., Ambrosio, L., and Nicolais, L. Continuous fibre reinforced polymers as connective tissue replacement. Composites Sci Technol **64,** 861, 2004.

52. Johnson, G.A., Tramaglini, D.M., Levine, R.E., Ohno, K., Choi, N.Y., and Woo, S.L. Tensile and viscoelastic properties of human patellar tendon. J Orthop Res **12,** 796, 1994.

53. Peltonen, J., Cronin, N.J., Avela, J., and Finni, T. *In vivo* mechanical response of human Achilles tendon to a single bout of hopping exercise. J Exp Biol **213,** 1259, 2010.

54. Svensson, R.B., Hansen, P., Hassenkam, T., Haraldsson, B.T., Aagaard, P., Kovanen, V., Krogsgaard, M., Kjaer, M., and Magnusson, S.P. Mechanical properties of human patellar tendon at the hierarchical levels of tendon and fibril. J Appl Physiol **112,** 419, 2012.

55. Hayami, J.W.S., Surrao, D.C., Waldman, S.D., and Amsden, B.G. Design and characterization of a biodegradable composite scaffold for ligament tissue engineering. J Biomed Mater Res Part A **92,** 1407, 2010.

Address correspondence to:
Qiang Zhou, PhD
Orthopaedics Department
Southwest Hospital
The Third Military Medical University
Chongqing 400038
China

E-mail: zqtlh@yahoo.com.cn

Xiumei Mo, PhD
College of Chemistry and Chemical Engineering
and Biological Engineering
Donghua University
Shanghai 201620
China

E-mail: xmm@dhu.edu.cn

This article has been cited by:

1. Jérôme Sohier, Pierre Corre, Christophe Perret, Paul Pilet, Pierre Weiss. Novel and Simple Alternative to Create Nanofibrillar Matrices of Interest for Tissue Engineering. *Tissue Engineering Part C: Methods*, ahead of print. [Abstract] [Full Text HTML] [Full Text PDF] [Full Text PDF with Links]